Computer-Aided Design 180 (2025) 103826

Contents lists available at ScienceDirect

Computer-Aided Design

journal homepage: www.elsevier.com/locate/cad

Research Paper

Interactive 3D structural design in virtual reality using preference-based topology optimization

Zhi Li, Ting-Uei Lee, Yi Min Xie *

Centre for Innovative Structures and Materials, School of Engineering, RMIT University, Melbourne, 3001, Australia

ARTICLE INFO

Dataset link: https://doi.org/10.25439/rmt.25469278.v1

Keywords:
Structural design
Virtual reality
Topology optimization
Subjective preference
Design exploration
Innovative structure

ABSTRACT

Innovative load-bearing structures often emerge from a fine balance between creative forms and engineering principles. While preference-based topology optimization methods have advanced structural design by considering designers' geometric preferences, they struggle with visualizing and editing complex 3D details crucial for diverse design options. To overcome this bottleneck, here we propose the improved bidirectional evolutionary structural optimization considering subjective preferences (ISP-BESO) method. This method introduces a similarity constraint that enables precise control over subjective preferences in optimized structures. Then, a design exploration strategy is proposed by integrating virtual reality (VR) with topology optimization for the interactive creation of desirable 3D structures. The strategy employs VR sculpting to offer immersive visualization and real-time feedback, guiding material redistribution during optimization. This workflow can iteratively produce innovative and efficient structures. Adjusting target similarity in ISP-BESO steers designs toward performance-driven or preference-driven outcomes. A museum design example demonstrates the practical potential of this strategy.

1. Introduction

Innovative load-bearing structures are typically designed not only to carry loads but also to possess unique geometric features that embody designers' creative ideas. However, the emphasis on creative expression may result in neglect of structural efficiency and fundamental engineering principles. Many structural optimization techniques have been developed to achieve specific objectives while satisfying certain constraints. These techniques include topology optimization, an effective strategy to automatically create innovative and efficient structures through redistributing the underutilized material, typically performed for stiffness maximization [1].

The bidirectional evolutionary structural optimization (BESO) method [2] is a widely used topology optimization technique that can redistribute the underutilized material to the most-needed locations by adding efficient or removing inefficient finite elements. In recent years, BESO has been increasingly used because of the availability of high-speed computers, efficient numerical algorithms, and limited material resources. Therefore, the BESO method has found diverse practical applications, including in additive manufacturing [3–7], bridge design [8–11], architectural design [12–18], and furniture [19–21].

According to Xie [13], optimized structures based purely on structural performance may be of low value, as they cannot always satisfy all design requirements, such as aesthetic quality. Recent studies have attempted to generate satisfactory structures through topology optimization considering subjective preferences (e.g., preferred geometric features). These preference-based topology optimization methods are achieved by applying appearance constraints [22,23], machine learning [24,25], image-text neural network [26], generative adversarial networks [27], subdomains [28], manually processing [29] or subjective weights [14]. These methods can yield multiple design options by adjusting parameters in a single design exploration. Then, designers must select a satisfactory design from these options. However, the selection process can be time-intensive, as finding solutions that satisfy all design requirements is often challenging [20]. Besides, relying on a single design exploration ignores that subjective preferences may be changed—often influenced by the solutions—leading to new inspirations [30]. Therefore, it is crucial for an effective design exploration process to allow designers the flexibility to update their subjective preferences [31].

Interactive topology optimization aims to involve the user in the optimization process, enabling real-time adjustments to design parameters, constraints, and aesthetic considerations. Hence, designers have more design freedom to guide topology optimization to generate desirable structures. For example, Li et al. [20,21] proposed the bidirectional evolutionary structural optimization considering subjective preferences

* Corresponding author.
E-mail address: mike.xie@rmit.edu.au (Y.M. Xie).

https://doi.org/10.1016/j.cad.2024.103826
Received 16 October 2024; Received in revised form 16 November 2024; Accepted 17 November 2024
Available online 30 November 2024

(SP-BESO) method by integrating interactive scoring and drawing systems. This method can convert the user inputs into subjective weights to guide the generation of 2D-optimized structures. However, as discussed by Yan et al. [14] and Li et al. [20], subjective weights easily dominate the formation of the optimized structures. This makes it difficult for users to accurately control the influence of subjective preferences by adjusting design parameters. Subsequent studies introduce drawing-based appearance constraints [32] and interactive feature size controls [33,34] into topology optimization to consider subjective preferences. Their methods can accommodate evolving subjective preferences in both 2D and 3D structural design by defining cuboid-shaped regions of interest (ROI). However, designers' preferences often include intricate geometric details, such as organic shapes and freeform curves, to show their creative ideas [20]. This necessitates more flexible interactive methods to fully capture and implement these nuanced preferences in 3D topology optimization. Additionally, the complexity of visualizing and modifying 3D models makes it challenging to develop such interactive methods. 3D topology optimization typically includes internal geometric details that are not visible or editable from the outside. Designers without strong spatial awareness often find it difficult to work with 3D structures on a 2D screen, adding further difficulty to 3D design exploration [35].

This paper proposes a novel preference-based topology optimization method by improving our previously developed SP-BESO method, named 'ISP-BESO'. The proposed method introduces a similarity constraint and 3D subjective weights, allowing users to accurately control the influence of subjective preferences on the optimized structures. We also propose a design exploration strategy that integrates virtual reality (VR) to create preferred 3D structures (see Fig. 3). In this VR environment, designers can intuitively observe and modify complex 3D geometries. They can start by sculpting a preferred model, which is then converted into subjective weights to guide material distribution in ISP-BESO for creating 3D structures. Designers can further refine preferences and execute optimization to efficiently explore the ideal structural design that satisfies both engineering and aesthetic needs.

The main contributions of this paper are summarized as follows:

- A novel preference-based topology optimization method, ISP-BESO, is proposed by introducing a similarity constraint and 3D subjective weights.
- A design exploration strategy is proposed by combining virtual reality with topology optimization.
- The sculpting–optimization workflow that can be executed repeatedly until the ideal design is found, achieving an iterative design exploration to fit evolved subjective preferences.
- A digital design tool, VR-BESO, is proposed to assist designers in 3D structural design using the proposed strategy.
- Computational design examples demonstrate that the proposed strategy can leverage the strengths of human insights and computational power to enhance the efficiency of design exploration and the quality of optimized structures.

The remainder of the paper is organized as follows: Section 2 introduces the SP-BESO method and the novel features of the proposed ISP-BESO method. Section 3 describes the details of the proposed design exploration strategy. Section 4 presents a parametric study, and Section 5 showcases a potential practical application of the proposed design exploration strategy, followed by a conclusion in Section 6.

2. ISP-BESO method

2.1. SP-BESO method

This proposed ISP-BESO method is developed by improving our previously developed SP-BESO method [20]. In the SP-BESO framework, for a given design domain discretized into N elements, the stiffness maximization (compliance minimization) problem under a volume constraint can be formulated as:

$$min: \quad C = \frac{1}{2}\mathbf{U}^T\mathbf{K}\mathbf{U} \tag{1a}$$

$$s.t.: \quad V^* = \sum_{i=1}^{N} v_i x_i \tag{1b}$$

$$x_i = x_{min} \text{ or } 1 \tag{1c}$$

where C, $\mathbf{U}$, and $\mathbf{K}$ represent the mean compliance, the global displacement vector, and the global stiffness matrix, respectively; V^* and v_i are the target structural volume and the volume of ith element e_i, respectively. A design variable x_i is used to determine whether e_i is solid ($x_i = 1$) or void ($x_i = x_{min} = 0.001$).

The material model of structural elements is determined as a function of the elemental density with penalization [1]:

$$E(x_i)^k = x_i^p E_0 \tag{2}$$

where $E(x_i)^k$ represents Young's modulus of the ith element at the kth iteration. E_0 is the design Young's modulus of structural elements. p is the penalty exponent. Unless otherwise stated, this study uses $p = 3$ [2].

The SP-BESO method is developed based on the BESO method. Their design variables are determined by the relative ranking of sensitivity numbers. Compared with the BESO method, the ith elemental sensitivity number, α_i, in SP-BESO is derived from both subjective preference and structural performance, corresponding to subjective weights, ω_i^s, and structural performance weights, ω_i^o. To ensure a comparable scale, normalization is applied to the calculation of α_i:

$$\bar{\omega}_i^s = \frac{\omega_i^s - \omega_{min}^s}{\omega_{max}^s - \omega_{min}^s} \tag{3a}$$

$$\bar{\omega}_i^o = \frac{\omega_i^o - \omega_{min}^o}{\omega_{max}^o - \omega_{min}^o} \tag{3b}$$

$$\alpha_i = \lambda\bar{\omega}_i^s + (1-\lambda)\bar{\omega}_i^o, \ \lambda \in [0,1] \tag{3c}$$

where ω_{min}^s and ω_{max}^s represent the minimum and maximum subjective weights, respectively. ω_{min}^o and ω_{max}^o are the minimum and maximum structural performance weights, respectively. λ is a user-defined design parameter within $[0,1]$, which controls the formation of the final topology to be performance-driven or preference-driven designs [20]. Note that when $\lambda = 0$, α_i does not include subjective preferences. In this case, the SP-BESO method is equivalent to the traditional BESO method.

ω_i^s is defined by the interactive systems [20]. For example, the drawing system requires designers to input a hand-drawn pattern representing subjective preferences. Then, ω_i^s can be calculated by the local color of the pattern:

$$\omega_i^s = \frac{\sum_{j=1}^{N_i^D}(1-col_j)}{N_i^D}, \quad col_j \in [0,1] \tag{4}$$

where N_i^D is the number of nodes in the ith element; col_j is the grayscale of the jth node on the hand-drawn pattern, ranging from 0 (black) to 1 (white). The calculation of ω_i^o is the same as the sensitivity calculation of the BESO method [2], which is computed as:

$$\omega_i^o = -\frac{1}{p}\frac{\partial C}{\partial x_i} = \begin{cases} \frac{1}{2}\mathbf{u}_i^T\mathbf{k}_i\mathbf{u}_i, & \text{when } x_i = 1 \\ \frac{x_{min}^{p-1}}{2}\mathbf{u}_i^T\mathbf{k}_i\mathbf{u}_i, & \text{when } x_i = x_{min} \end{cases} \tag{5}$$

where $\mathbf{k}_i$ is the ith elemental stiffness matrix, and $\mathbf{u}_i$ is the ith elemental displacement vector.

To avoid checkerboard and mesh dependency problems, a filtering procedure is applied to smooth the raw sensitivity number, as described by [36].

$$\tilde{\alpha}_i = \frac{\sum_{j=1}^{N}(r_{min} - r_{ij})\alpha_i}{\sum_{j=1}^{N}(r_{min} - r_{ij})} \tag{6}$$

where $\tilde{\alpha}_i$ is the filtered sensitivity number, r_{min} is the filter radius, and r_{ij} represents the distance between the centroids of elements i and j.

To improve the convergence of the SP-BESO method, the current and historical sensitivity numbers can be averaged using the following equation [2]:

$$\hat{\alpha}_i = \frac{\tilde{\alpha}_i{}^k + \tilde{\alpha}_i{}^{k-1}}{2} \tag{7}$$

where $\hat{\alpha}_i$ is the averaged sensitivity number.

Before elements are added to or removed from the current design, the target volume for the next iteration, $\mathbf{V}^{k+1}$, needs to be given because the volume constraint can be greater or smaller than the volume of the initial guess design. The evolution of the volume can be represented by

$$\mathbf{V}^{k+1} = \mathbf{V}^k(1 \pm ER) \tag{8}$$

where $\mathbf{V}^k$ denotes the current volume. ER represents the evolutionary rate, which controls how much material is added or removed in each iteration, aiding convergence toward the optimized structure.

Next, the bisection method is used to update the current design by adding or removing elements according to $\hat{\alpha}_i$ [37]. The optimization process is repeated until the following convergence criteria are satisfied [38]:

$$\frac{|\sum_{m=1}^{M}(C_{k-m+1} - C_{k-M-m+1})|}{\sum_{m=1}^{M} C_{k-m+1}} \leq \tau \tag{9}$$

where $M = 5$ is an integer number and $\tau = 0.001$ is the allowable convergence error. Here, M is set as 5, meaning stable compliance values are checked in the last ten iterations.

2.2. Improvement of SP-BESO method

As introduced in Section 1, the original SP-BESO method is limited. Inspired by the existing methods [23,32,39], the proposed ISP-BESO method introduces a similarity constraint and an automatic update scheme for the design parameter λ in Eq. (3)(c) to solve the limitations. The improvement allows designers to precisely control the importance of subjective preferences by defining the similarity constraint, eliminating the need to manually adjust λ. Moreover, the new ISP-BESO method extends the SP-BESO method to three-dimensional applications by allowing designers to input a preferred 3D model, D. This model is then used to calculate 3D subjective weights through a distance field. Then, these weights serve as subjective preferences to guide topology optimization in generating preferred 3D designs. Compared to the SP-BESO method, which is limited to 2D, the 3D-capable ISP-BESO method is more practical in real-world design scenarios.

Mathematically, the compliance minimization problem of the proposed ISP-BESO method is described as follows:

$$min: \quad C = \frac{1}{2}\mathbf{U}^T\mathbf{K}\mathbf{U} \tag{10a}$$

$$s.t.: \quad V^* = \sum_{i=1}^{N} v_i x_i \tag{10b}$$

$$S = \frac{\sum_{i=1}^{N} s_i x_i}{\sum_{i=1}^{N} s_i} \geq S^* \tag{10c}$$

$$x_i = x_{min} \text{ or } 1 \tag{10d}$$

$$s_i = 0 \text{ or } 1 \tag{10e}$$

where S and S^* represent the current and target similarity, respectively. The similarity used in this study is defined by measuring the overlapping rate between the current optimized structure and the preferred model D. s_i represents the inclusion status of the ith element e_i, which is used to determine whether e_i is included ($s_i = 1$) or excluded ($s_i = 0$) by D.

To integrate subjective preferences, the subjective weight ω_i^s in Eq. (4) is redefined as the shortest distance from each elemental centroid to the boundary of D:

$$\omega_i^s = \begin{cases} Dist(c_i, \partial D), & \text{if } c_i \in D \\ 0, & \text{otherwise} \end{cases} \tag{11}$$

where c_i is the centroid of ith element, ∂D represents the boundary of D, and $Dist(c_i, \partial D)$ is the shortest distance from c_i to ∂D.

To calculate elemental sensitivity numbers, ω_i^s is normalized into $\bar{\omega}_i^s$ by using Eq. (3)(a). The elemental sensitivity number α_i^D used in the ISP-BESO method is defined as:

$$\alpha_i^D = \hat{\lambda}\bar{\omega}_i^s + (1 - \hat{\lambda})\bar{\omega}_i^o, \ \hat{\lambda} \in [0, 1] \tag{12}$$

where $\hat{\lambda}$ is a dynamic weight from 0 to 1 that controls the influence of the subjective weights. Before the optimization, $\hat{\lambda}$ is initialized to 0. Its dynamic update scheme in each iteration is defined as follows:

$$\hat{\lambda}_{k+1} = \hat{\lambda}_k + \frac{(S^* - S)}{S^*} \tag{13}$$

where $\hat{\lambda}_k$ and $\hat{\lambda}_{k+1}$ represent the dynamic weight in the kth iteration and $(k+1)$-th iteration, respectively. Note that the dynamic weight ranges from 0 to 1. Therefore, $\hat{\lambda}_{k+1}$ is set to 0, if $(S^* - S)/S^*$ is less than 0; and $\hat{\lambda}_{k+1}$ is set to 1, if $(S^* - S)/S^*$ is greater than 1.

Together, by calculating the new sensitivity numbers α_i^D and executing the remaining steps (Eqs. (7)–(9)), an optimized design can be obtained. At the end of each iteration, the constraints in Eqs. (10)(b) and (10)(c) are checked, and $\hat{\lambda}$ is updated using Eq. (13). Iteratively executing topology optimization ensures that the volume and similarity constraints, as well as the convergence condition, are satisfied, resulting in a satisfactory design. If this design is still deemed unsatisfactory after subjective evaluation, the designer can initiate a new round of design exploration by refining preferences, recalculating the subjective weights and inclusion status, and performing subsequent topology optimization until the resulting design meets all requirements.

It should be noted that the optimization process may locally produce overly high subjective weights, which lead to the formation of suspended components and error displacement values. To solve this issue, the breadth-first search (BFS) algorithm is included in the ISP-BESO method to group all interconnected elements [40]. Then, the largest cluster is preserved, while isolated suspended components in smaller groups are removed. This strategy is applied as an extra step in each iteration, ensuring that the structural design remains continuous and reasonable.

The computational workflow of the proposed ISP-BESO method is summarized in Fig. 1. The new features are highlighted in this workflow, including calculating inclusion status, calculating subjective weights, removing isolated elements, and checking similarity constraints.

3. Design exploration in virtual reality

Based on the ISP-BESO method, a VR-based design exploration strategy is proposed. VR devices, generally including a head-mounted display (HMD) and two handheld controllers, enable designers to perform operations based on body motion, offering an intuitive way to interact with the virtual environment. Importantly, the immersive environment is particularly beneficial for inexperienced designers, as it assists them in understanding complex 3D details and refining their subjective preferences.

This section describes the computational workflow of the proposed design exploration strategy (see Fig. 2). Four sequential steps are involved within a single design cycle, including VR sculpting (Step 1), initialization (Step 2), topology optimization (Step 3), and smoothing (Step 4), detailed in Sections 3.1–3.4, respectively. Each cycle gives an optimized structure that aligns with the current subjective preferences. However, Steps 1–4 can be iteratively repeated to update subjective preferences, creating a series of desired structures that progressively

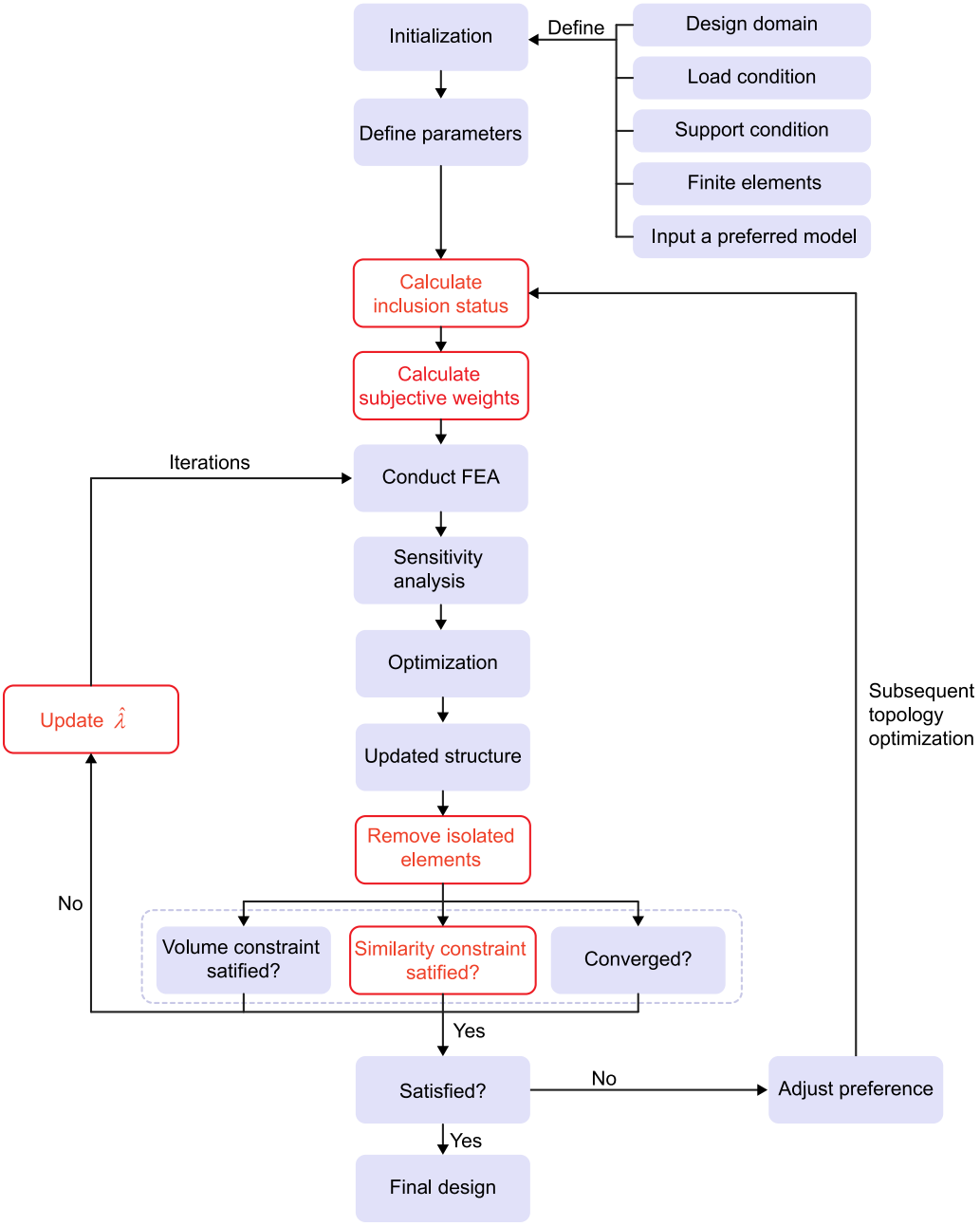

Fig. 1. Computational workflow of the ISP-BESO method.

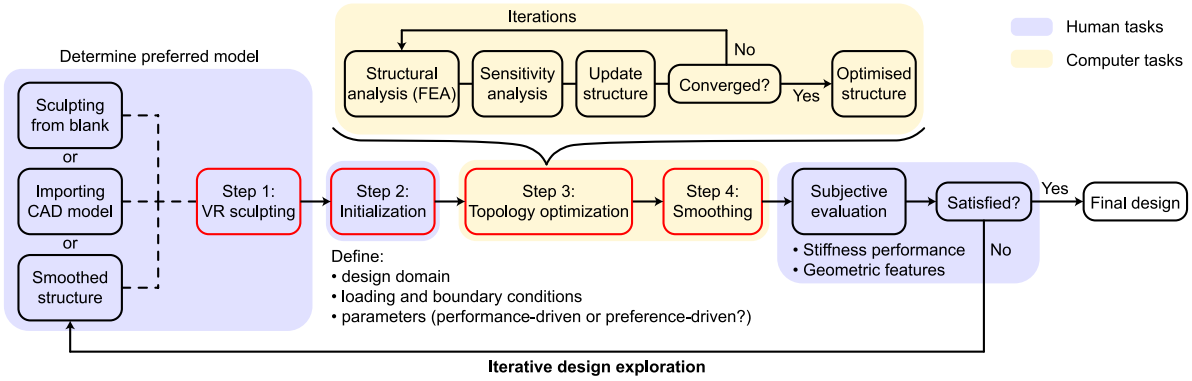

Fig. 2. Computational workflow of the proposed design exploration strategy.

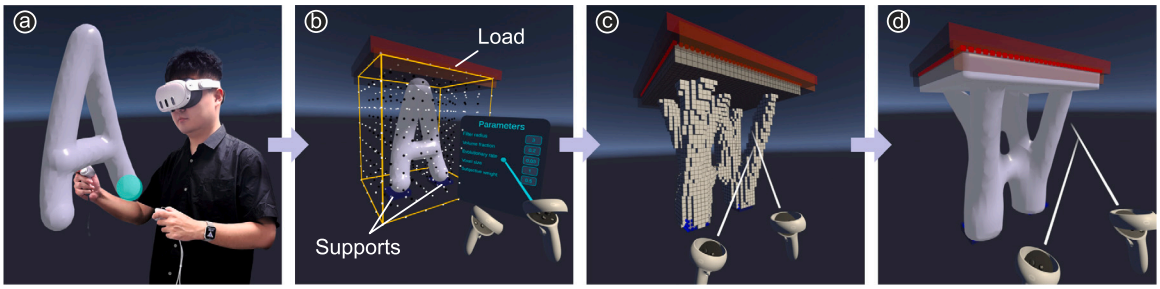

Fig. 3. A single design cycle within the computational workflow of the proposed design exploration strategy: (a) Stage 1: VR sculpting; (b) Stage 2: initialization; (c) Stage 3: topology optimization; (d) Stage 4: smoothing.

match these evolving preferences. This design exploration strategy establishes a productive human–computer collaboration to improve the efficiency of design exploration and the quality of optimized structures (see Sections 3.5 and 3.6). Furthermore, we have developed a digital design tool—virtual reality-based bidirectional evolutionary structural optimization (VR-BESO)—to implement the proposed strategy (see Section 3.7). All examples presented in this paper have been created using VR-BESO. This newly developed software and its documentation have been made publicly available [41].

3.1. Stage 1: VR sculpting

Step 1 utilizes VR sculpting to help designers transform their creative ideas into tangible 3D geometries in a virtual environment, as shown in Fig. 3(a). This process offers a direct and intuitive way for designers to express their subjective preferences. VR sculpting differs significantly from traditional flat-screen design interfaces, offering six degrees of freedom to simulate a real-life sculpting experience [42,43]. This technology typically includes various brush tools for drawing, building up, and removing material, offering extensive design freedom. Designers can shape their ideal geometries by waving the two handheld controllers, making the process accessible to those without 3D modeling experience.

In Step 1, designers can import external 3D geometries created with other computer-aided design (CAD) software (e.g., Rhinoceros [44]). This capability is important, as it allows designers to bypass the need to start sculpting from blank. Instead, they can begin by modifying and refining preexisting designs. The imported design is first converted into an editable model using advanced surface reconstruction techniques [45]. Designers can then utilize VR sculpting tools to add new features or remove unwanted parts, guided by their artistic intuitions or preferences. This capability conserves time that would otherwise be spent sculpting models from blank and allows designers to concentrate on refining their subjective preferences. The implementation of VR sculpting can be found in the Appendix.

3.2. Stage 2: initialization

While VR sculpting (Step 1) significantly eases the expression of subjective preferences, there is a risk that excessive design freedom might lead designers to focus too much on creative ideas and neglect fundamental engineering principles. Structural optimization becomes a crucial step in the design exploration process to ensure that the sculpted models have practical value. Before executing this optimization, the initial settings must be established to clearly define the design optimization problem.

In Step 2 (see Fig. 3(b)), the initial task is to determine the size of the design domain (i.e., the space in which materials can be redistributed). Designers can use the handheld controllers to adjust the dimensions of this design domain to align with specific design requirements; the adjusted bounding box is marked by a cubic frame in Fig. 3(b). Subsequently, designers can define the support and load conditions. In Fig. 3(b), a uniformly distributed load is applied on top of the design domain, represented by the rectangular box, and two fixed supports are set at the base, represented by two dark boxes. Finally, Step 2 concludes by inputting optimization parameters through a virtual number pad. These parameters include the filter radius, volume fraction, evolutionary rate, voxel size, and subjective weight. Notably, the 'subjective weight' parameter actually refers to the target similarity introduced in the ISP-BESO method. However, we use 'subjective weight' in VR-BESO software so that users can understand it more easily.

3.3. Stage 3: topology optimization

Step 3 (see Fig. 3(c)) performs the proposed ISP-BESO method (see Section 2.2). Initially, the sculpted model is transformed into subjective weights by computing a distance field. These weights are then incorporated into the sensitivity analysis; they play a pivotal role in the optimization procedure determining materials' addition or removal. Moreover, by adjusting 'subjective weight' (the target similarity in ISP-BESO), designers are allowed to control the formation of final structural topologies to be performance-driven or preference-driven. This feature indicates that our topology optimization enables the sculpted models to be computationally refined into high-performance structures.

3.4. Stage 4: smoothing

The proposed ISP-BESO method is based on finite element analysis (FEA), requiring the continuous design domain to be discretized into finite element meshes to represent the given materials. Therefore, optimization results possess zig-zag boundaries formed from straight element edges [46,47]. These boundaries, and hence the design resolution, are determined by the number of elements. A resolution that is not sufficiently fine could affect how designers perceive and define their subjective preferences. Step 4 is an additional smoothing step to improve the aesthetic quality of the optimization result obtained from Step 3 (see Fig. 3(d)).

The authors previously developed the smoothing algorithm utilized in this study based on a pre-built lookup table [48]. Notably, the smoothed model can be exported to external CAD software. This capability grants designers considerable flexibility: they can further modify the design for various purposes, including as a new input for Step 1, for rendering, or to meet specific manufacturing requirements.

3.5. Iterative design exploration

A single design exploration may not fulfill all design requirements, as designers often develop new preferences during the exploration process [20]. Our proposed design exploration strategy offers flexibility by allowing designers to modify the results from Steps 1–4 and redesign through these steps again. This iterative approach ensures that the evolving subjective preferences are continually updated.

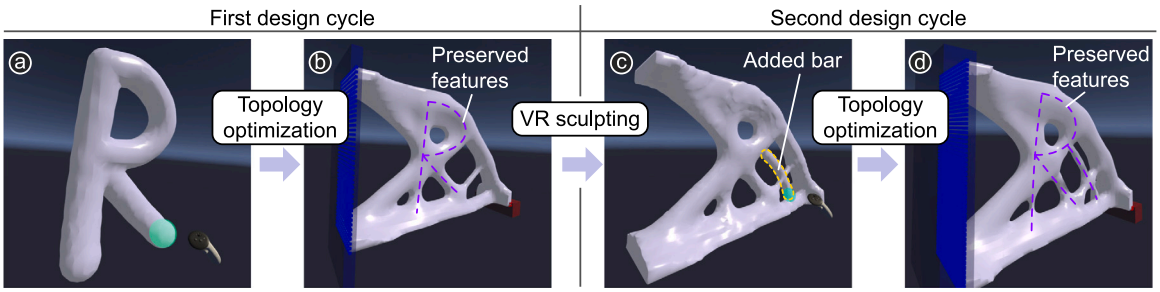

Fig. 4. Iterative design exploration: (a) sculpting a preferred model; (b) obtaining an optimized topology via a single design cycle; (c) adding a bar to the current design through VR sculpting; (d) generating a new optimized design.

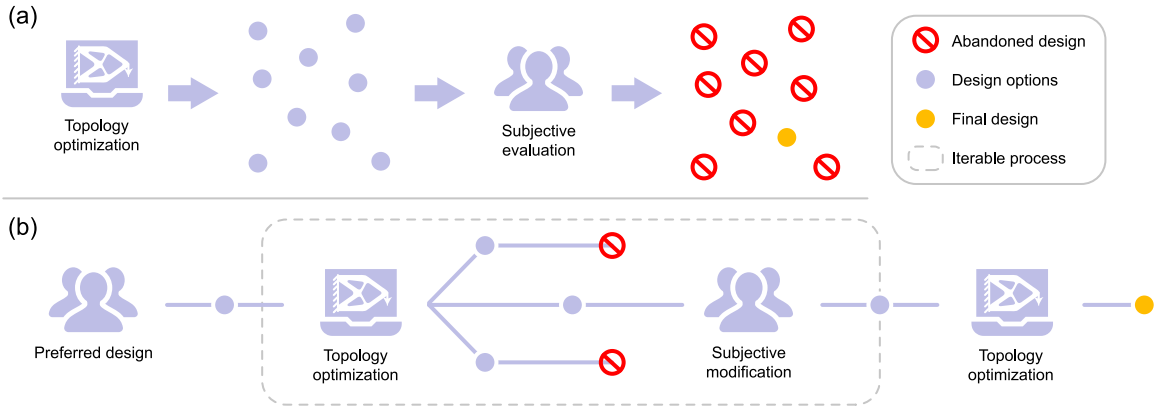

Fig. 5. (a) Single design exploration versus (b) the proposed iterative design exploration.

The iterative design exploration is demonstrated more clearly in Fig. 4. Figs. 4(a) and 4(b) represent the sculpted models before and after optimization, respectively. Designers can manually add or remove specific parts from the optimization result, as shown in Fig. 4(c). These modifications significantly influence the subsequent topology optimization, as shown in Fig. 4(d). Designers can also undertake a series of iterative design explorations by alternately updating the preferred geometric features and executing topology optimization. This process is repeated until the subjective preferences are refined to achieve a final design that best meets all requirements.

3.6. Effective design exploration explained

Unlike traditional single-design exploration strategies (see Fig. 5(a)), the proposed strategy (see Fig. 5(b)) eliminates the extensive evaluation tasks involved in selecting a design from a wide array of often unsatisfactory options [20]. The proposed new approach empowers designers to participate in and guide the design process effectively.

In fact, the key contribution in this study is to establish a productive human–computer collaboration by integrating VR sculpting and topology optimization. This collaboration enables user preferences to directly guide topology optimization, fostering the creation of innovative structures. VR sculpting allows designers to express their subjective preferences; Topology optimization ensures the structural performance of these innovative structures. This synergistic relationship effectively leverages the unique strengths of human insight and computational power, thereby enhancing the efficiency of design exploration and the quality of optimized structures.

3.7. VR-BESO demonstration

The VR-BESO design tool is developed using both C++ and C# programming languages. The C++ part provides a CPU-parallel optimization kernel, which is achieved based on open-source dependencies and the existing topology optimization codes [37,49,50]. The dependences used in the computational kernel include the MKL PARDISO solver [51] and the Eigen linear algebra library [52]. The C# part relies on Unity3D and Meta Quest SDK to implement a graphical user interface and an interactive system in the VR space [53,54].

The hardware requirements of VR-BESO include the HMD and two handheld controllers of the Meta Quest 3 [54] and a personal computer. The VR device is used to display and interact with 3D geometries. However, due to the limited computational resources of VR devices, a high-performance personal computer with an Intel i9-13900KF 3.00 GHz processor is employed to deal with computationally demanding tasks, such as executing topology optimization and smoothing the optimized topologies.

In VR-BESO, the initial design scene is a dark virtual space, as shown in Fig. 6(a). Designers wearing a VR headset can turn their heads to observe the geometric details of the 3D model from different angles. The interaction between the virtual space and the real world is implemented by the two handheld controllers. Fig. 6(b) shows the structure of the two controllers. Designers can operate the physical buttons on the two real controllers to perform basic actions, such as selecting, moving, rotating, and scaling 3D geometries, as shown in Fig. 6(c).

Moreover, the left controller can call a floating panel that includes intractable buttons and input fields. When the right controller points toward the floating panel, a white ray emanates from the controller and hits the floating panel (Fig. 6(a)). Pressing the index trigger on the right controller can interact with these buttons and input fields. Designers can also switch the pages of the floating panel by pushing the thumbstick on the left controller. The floating panel includes three different pages: ‘Modeling’, ‘Parameters’, and ‘Optimization’. All features used in the proposed design exploration strategy are included in the pages. In detail, the functions of the three pages are described as follows:

- **‘Modeling’ page**: It has brush tools and input/output (I/O) functions, allowing designers to draw, erase, import, and export their creative 3D models by moving controllers.

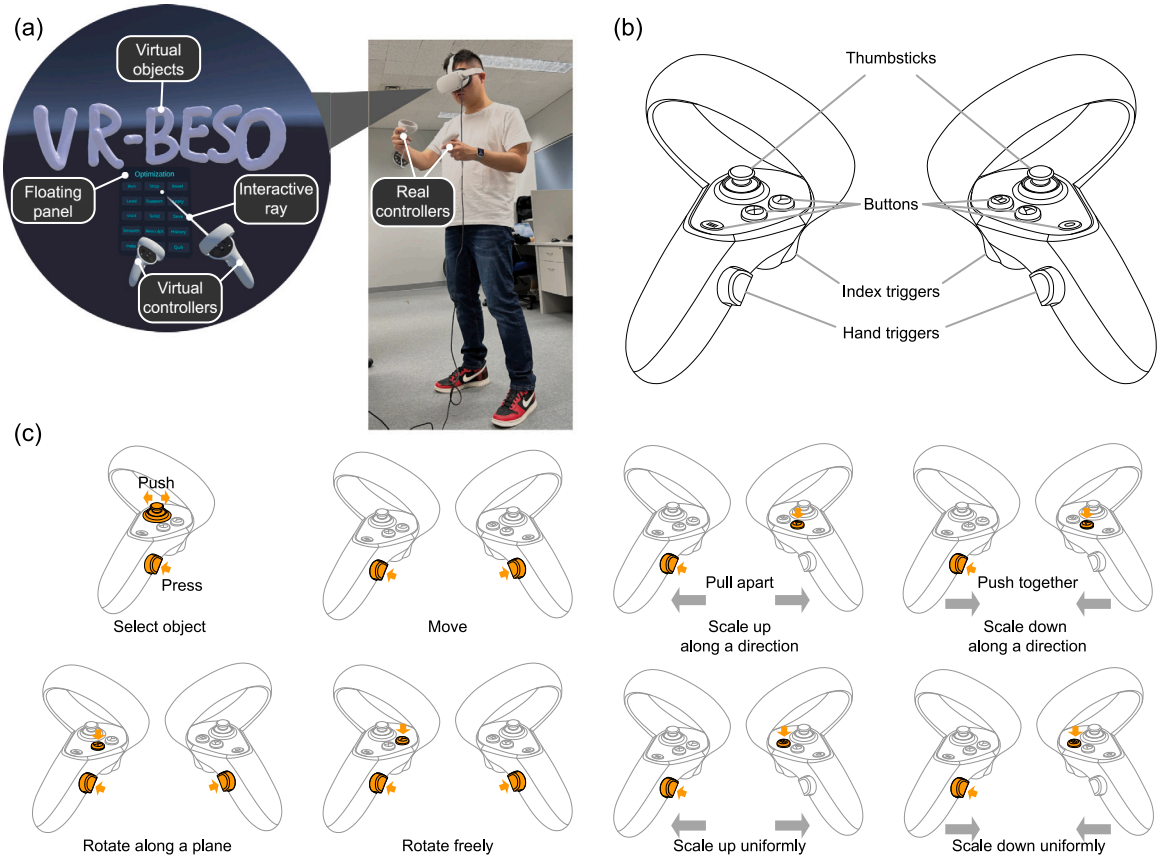

Fig. 6. The user interface and the interactive operations of VR-BESO: (a) operating 3D models in a virtual space; (b) the structure of two controllers; (c) interactive operations for transforming 3D geometries.

- **'Parameters' page**: It controls the filter radius r_{min}, volume fraction V^*, voxel size (controls the number of elements in the X, Y and Z directions), and subjective weight (the target similarity, S^*).
- **'Optimization' page**: It includes buttons to set and control the optimization process, such as 'Run', 'Stop', 'Reset', 'Load', 'Support', 'Apply', 'Solid', 'Void', 'Smooth', 'Save', 'Info', 'History', and 'Resculpt'. Note that 'Solid' and 'Void' buttons can define constant solid elements ($x = 1$) and constant void elements ($x = x_{min}$), respectively [55].

By operating the functions on the floating panel, designers are able to conduct the proposed design exploration strategy.

4. Parametric study

A parametric study is conducted to investigate the effect of varying S^* on the formation of the resulting structural topology. Here, the design optimization problem of the parametric study is the classic 3D short cantilever [2]. The design domain is 80 mm long × 20 mm wide × 50 mm tall, discretized into 80,000 cubic elements. A point load, $F = -1$ N, is applied at the center of the free end. A fixed boundary condition is assigned behind the whole cantilever. The material used in this study is assumed to be isotropic and linear elastic, with Young's modulus of $E_0 = 1$ MPa and Poisson's ratio of $nu = 0.3$. BESO parameters are: $ER = 3\%$, $V^* = 15\%$, and $r_{min} = 3$ mm. Inspired by the shape of a butterfly, we designed a 3D geometry as the preferred model, as shown in Fig. 7(a). This model was initially created through VR sculpting and then refined in the Rhinoceros CAD software [44].

This study uses five different S^* to generate topologically different solutions, including 0.5, 0.6, 0.7, 0.8, and 0.9. Each solution is compared with two reference designs (Ref. 1 and Ref. 2). Ref. 1 (see Fig. 7(b)) is the original BESO result obtained without considering subjective preferences; it considers only structural performance. Ref. 2 (see Fig. 7(c)) is the extremely preference-driven design ($S^* = 1$), obtained by redistributing the given materials to the preferred model. This study uses the mean compliance ratio, C^* to quantify the differences in structural performance with Ref. 1. Specifically, $C^* = C'/C_{Ref.1}$, where C' and $C_{Ref.1}$ represented the mean compliance values of the given solution and Ref. 1, respectively.

Topology optimization results are summarized in Fig. 7(d), with the evolutionary histories shown in Fig. 7(e), measurement results of C^* are detailed in Fig. 7(f), and the variations of $\hat{\lambda}$ and S during the optimization are shown in Figs. 7(g) and 7(h), respectively. It can be found that increasing S^* from 0.5 to 0.9 leads to a noticeable rise in C^*. This trend suggests that a lower S^* tends to produce structures with performance characteristics more aligned with Ref. 1. Since more materials can be distributed to efficient areas as S^* decreases. Therefore, designers can adjust S^* according to their design requirements, effectively guiding the formation of the final structures toward performance-driven or preference-driven.

Moreover, observing the variations of $\hat{\lambda}$ and S (see Figs. 7(g) and 7(h)) can provide insights into the reasons behind the performance improvement. In the early stages of optimization, the proposed method prioritizes structural performance by rapidly decreasing S, allowing it to quickly approach a shape close to the optimized solution. This rapid reduction in the early phase ensures that the final result does not deviate too far from the optimized solution. Once S reaches the target similarity for the first time, the optimization process begins to balance subjective preferences and structural performance, causing $\hat{\lambda}$ to oscillate significantly. As the optimization progresses, these oscillations gradually reduce, and $\hat{\lambda}$ stabilizes at a higher value. Consequently, S

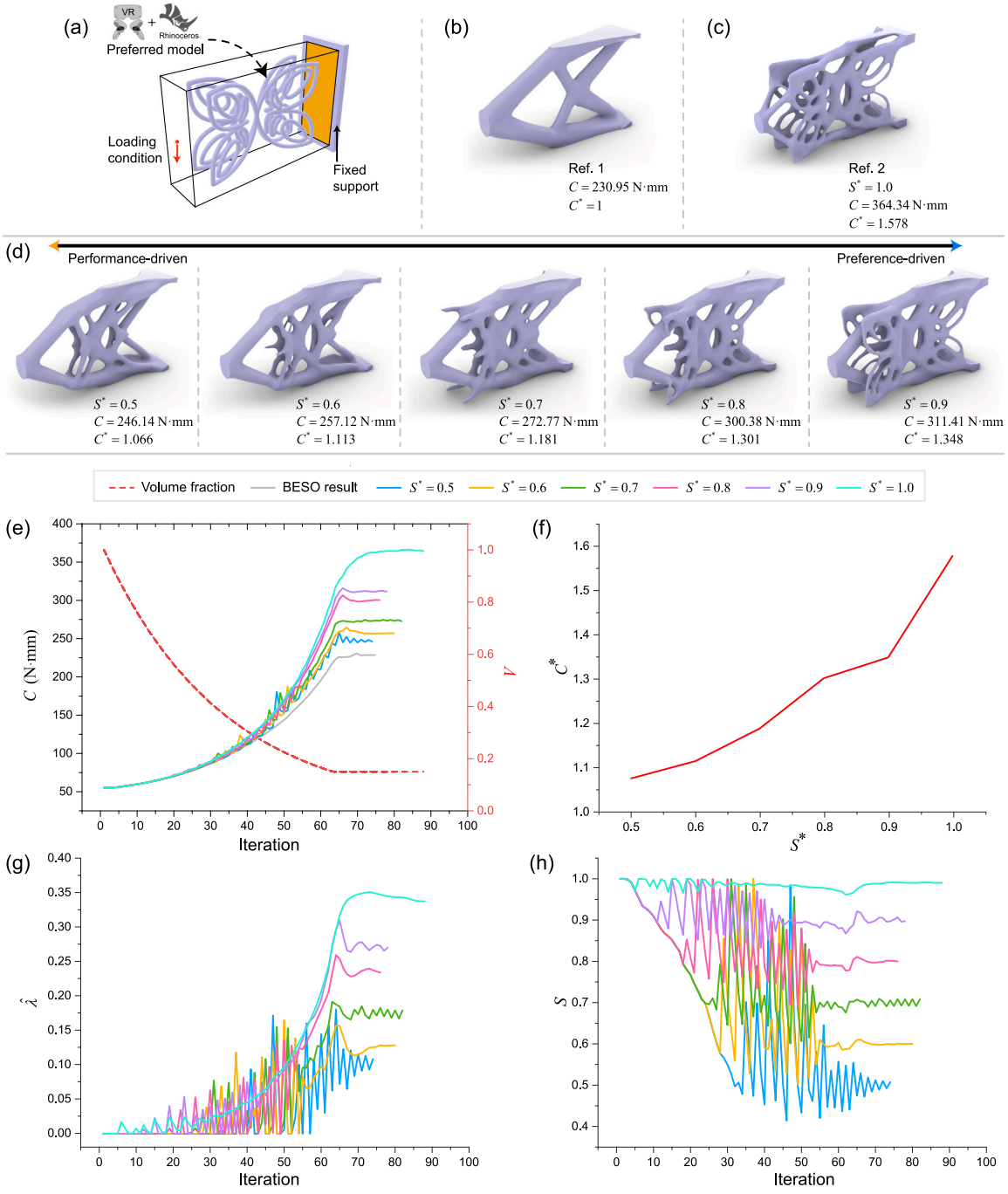

Fig. 7. Investigation of the influence of S^* on optimization results using the 3D cantilever example: (a) initialization and the preferred model created by VR sculpting and Rhinoceros [44]; (b) extremely performance-driven design (Ref. 1); (c) extremely preference-driven design (Ref. 2); (d) five designs obtained using different S^*; (e) evolutionary histories; (f) variation of C^* with respect to S^*; (g)–(h) variations of $\hat{\lambda}$ and S with respect to the iteration steps.

also stabilizes and eventually converges to S^*, ensuring that the final design meets both performance and similarity targets.

It is noted that the initial input geometry and parameters can lead to minor oscillations in both $\hat{\lambda}$ and S, as observed in Fig. 7 for cases with $S^* = 0.5$ and $S^* = 0.7$. These oscillations result from the algorithm's trade-offs on whether to retain certain overhanging bars. However, as the amplitudes of oscillations in $\hat{\lambda}$ and S gradually decrease, the optimization algorithm consistently finds a solution that also satisfies the constraints (see Eqs. (10)(b) and (10)(c)) and the compliance convergence condition (see Eq. (9)). This outcome demonstrates the robustness of the proposed method; even when the input geometry differs significantly from the optimized solution (e.g., the butterfly shape in Fig. 7), the proposed ISP-BESO is still capable of reaching a convergent result.

The computational resources required for the proposed ISP-BESO method are nearly equivalent to those of the traditional BESO algorithm. As shown in Fig. 7(e), the introduction of the similarity constraint does not significantly increase the number of iterations required for convergence. Additionally, the time spent per iteration remains consistent with the traditional BESO algorithm because the integration of subjective preferences is a linear weighting method (see Eq. (12)), which does not increase algorithmic complexity. As a result, the overall computational resource requirements for this algorithm are comparable to those of traditional BESO, even with the added flexibility

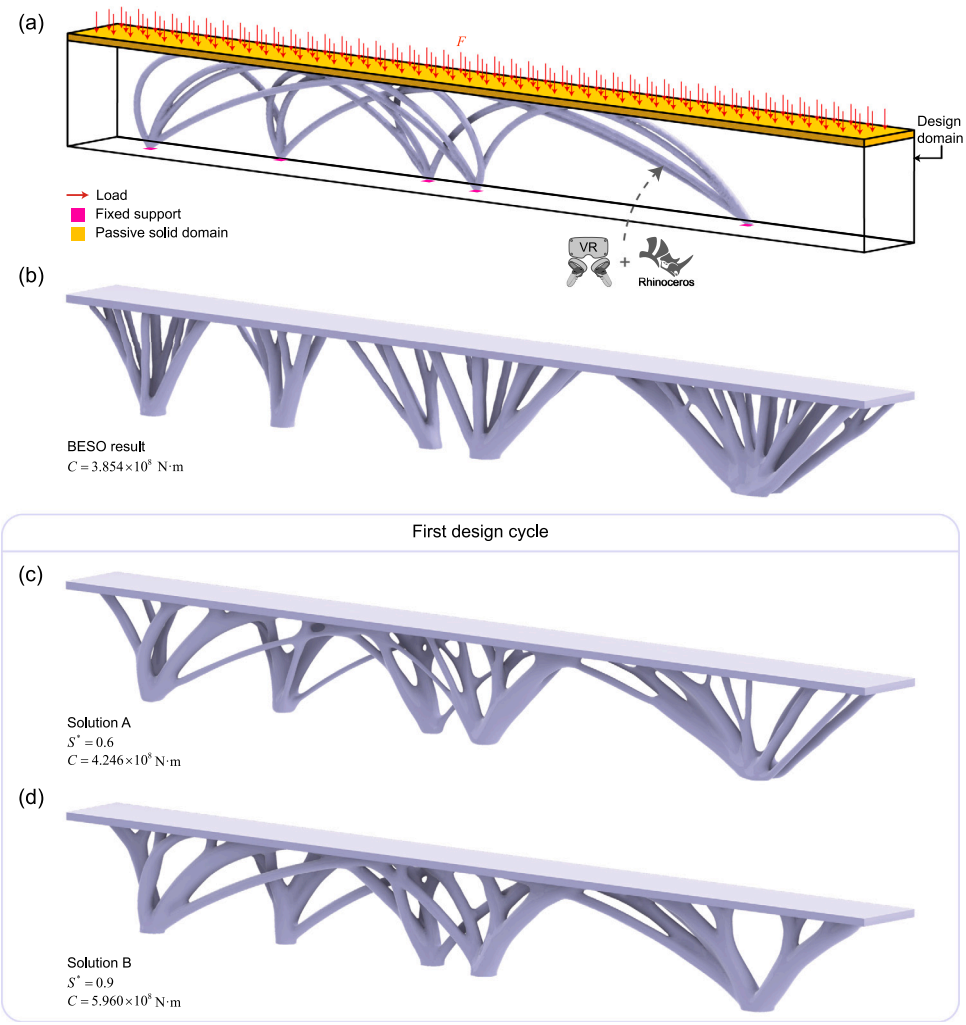

Fig. 8. The first design cycle of a museum design: (a) problem settings and the preferred model created by VR sculpting and Rhinoceros [44]; (b) reference design generated by the BESO method; (c) Solution A with $S^* = 0.6$; (d) Solution B with $S^* = 0.9$.

of adjusting subjective preferences within the optimization process. Due to the efficiency, the proposed ISP-BESO method can run smoothly on VR devices, supporting real-time interaction and iterative refinement in an immersive environment.

5. Potential application

Figs. 8–10 use a 3D museum design to demonstrate the potential practical applications of the proposed design exploration strategy. The problem settings of the museum design are inspired by the well-known Qatar National Convention Center, which was designed by the famous architect Arata Isozaki and his collaborators [56]. A cuboidal bounding box of 200 m long × 15 m wide × 22 m tall, which contains a layer of 1.5 m thick passive solid domain on the top and a design domain underneath, is discretized into 528,000 0.5 m cubic elements, as shown in Fig. 8(a). A uniformly distributed load, $F = -10000\ N/m^2$, is applied to the passive solid domain. Five rectangular fixed supports are applied at the base. The material used in this application is assumed to be isotropic and linear elastic, with Young's modulus of $E_0 = 30$ GPa and Poisson's ratio of $nu = 0.3$. BESO parameters are: $ER = 2\%$, $V^* = 12\%$, and $r_{min} = 1.5$ m.

The subjective preference model in this application is defined as ten arches, created through VR sculpting and refined using Rhinoceros CAD software [44]. These arches connect five rectangular supports to guide topology optimization to produce an overall structure. Fig. 8(b) shows the BESO result without considering subjective preferences, which is used as a reference design to measure the performance loss of the produced solutions. The goal of this application is to generate a structural design that retains most of the geometric features of the preferred model while avoiding the creation of overly slender bars and maintaining a high level of structural performance as much as possible.

Figs. 8(c) and 8(d) show the outcomes of the initial design cycle, showcasing two innovative structures (Solutions A and B). They are optimized using different values of S^*, 0.6 and 0.9, respectively. In this design cycle, Solution B may be chosen as the preferred design because it maintains subjectively preferred features while avoiding the generation of complex and slender bars. In contrast, Solution A produces too many slender bars. Despite its superior structural performance, the increased slender bars necessitate more intricate nodes, leading to higher manufacturing complexity and costs.

In the second design cycle (see Figs. 9(a) and 9(b)), this study wishes to improve the structural performance of Solution B. To this end, we remove four arc-like bars (marked red in Fig. 9(a)) by VR sculpting and set the modified geometry as the new preferred model. Then, we rerun the optimization using a relatively high value of $S^* = 0.95$ to ensure that the newly updated geometric features effectively influence the outcome. The optimization result is denoted as Solution C, which successfully includes all updated modifications. Besides, Solution C has a better structural performance than the preferred solution from the previous design cycle (Solution B). With both solutions incorporating

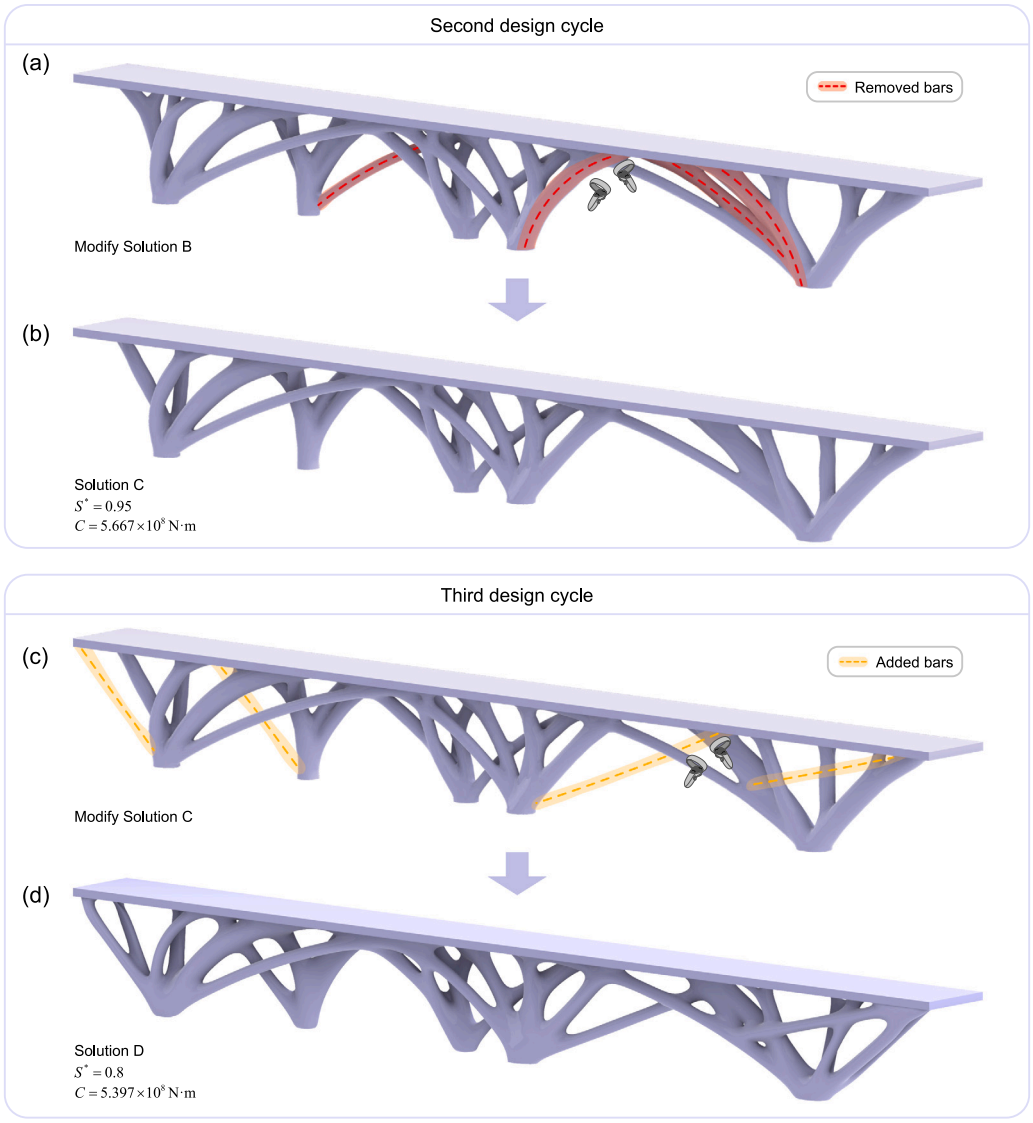

Fig. 9. The second and third design cycles of the museum design: (a) modification of Solution B; (b) Solution C with $S^* = 0.95$; (c) modification of Solution C; (d) Solution D with $S^* = 0.85$.

the preferred model, they emerge as strong contenders for the final design.

After a thorough subjective evaluation of the shapes of Solutions B and C within the VR environment, it can be concluded that Solutions B and C seem overly simplistic. Therefore, a third design cycle (see Figs. 9(c) and 9(d)) is performed or this new round, Solution C is modified by adding four new straight bars to support the roof, aiming to further enhance the structural efficiency. Then, the modified Solution C is selected as the preferred model to guide topology optimization. The optimized result, Solution D, achieved with $S^* = 0.8$, not only presents a more visually appealing design but is also 9.45% stiffer than Solutions B and 4.76% stiffer than Solution C, respectively. Based on these improvements, Solution D is selected as the final design for the 3D museum example, and its rendering for potential practical application is shown in Fig. 10.

This museum design demonstrates the benefits of an iterative design exploration approach grounded in human–computer collaboration. Through this process, designers actively shape the optimization results by inputting their preferred geometric features, which the algorithm then accommodates and enhances. The structural solution in each iteration may include unexpected bars due to the consideration of structural performance. It reveals that the algorithm's capacity to integrate additional bars when necessary not only improves the overall structural efficiency but also prevents subjective preferences from leading to overly inefficient structural designs. Moreover, these unexpected solutions may inspire further refinement of designers' subjective preferences, enabling designers to iteratively balance aesthetic intentions with structural functionality. Through each design iteration, designers thus gain opportunities to create a structure that fulfills both structural efficiency and artistic vision, and finally achieve an outcome that embodies both engineering integrity and creative expression. This approach highlights the synergy between algorithmic capabilities and designers' creativity, ultimately expanding the range and quality of solutions available in complex structural design.

It should be noted that the Qatar National Convention Center was constructed with a hollow structure, which differs from our assumption of a solid structure in topology optimization. This museum design was made primarily to demonstrate the applicability of our optimization method, rather than to suggest the construction details of the real building.

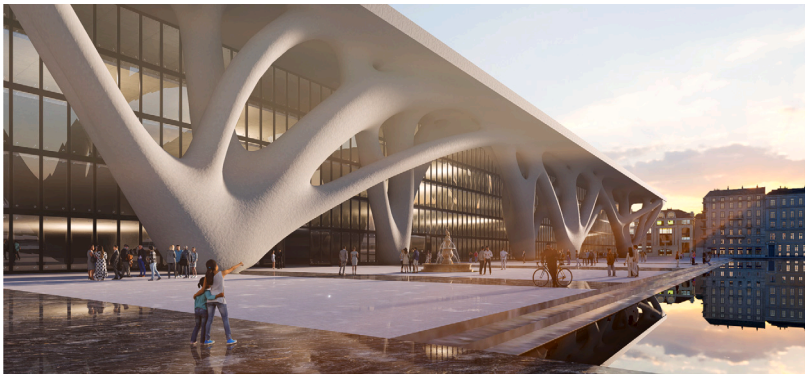

Fig. 10. Rendering of the museum design.

6. Conclusion

In this study, we have proposed a new preference-based topology optimization method, named ISP-BESO method. This method introduces a similarity constraint and 3D subjective weights, allowing users to accurately control the influence of subjective preferences on the 3D optimized structures. We have also developed a novel design exploration strategy that integrates VR and topology optimization. The integration of VR provides designers with an intuitive, interactive, and immersive platform for observing and editing 3D geometries. Designers can use VR sculpting to transform their creative ideas directly into 3D models. The sculpted models can represent their subjective preferences and influence material redistribution in the topology optimization process. Importantly, we emphasize that the sculpting–optimization workflow can be repeated in multiple cycles, creating various innovative and efficient structures that reflect designers' subjective preferences. Our newly developed digital design tool, VR-BESO, which implemented the proposed exploration strategy and generated all examples in this paper, is publicly available. Our findings indicate that by adjusting the target similarity of ISP-BESO, the optimization process can control the generated structural form to be either performance-driven or preference-driven. This flexibility enables the optimized structures to meet engineering principles and aesthetic preferences. Further, a museum design is conducted to highlight the practical applications of the proposed iterative design exploration strategy. The proposed strategy, coupled with VR-BESO, can effectively harness the strengths of human creativity and computational power to enhance the efficiency of design exploration and the quality of optimized structures.

CRediT authorship contribution statement

Zhi Li: Writing – original draft, Visualization, Validation, Software, Methodology, Data curation, Conceptualization. **Ting-Uei Lee:** Writing – review & editing, Supervision, Methodology, Conceptualization. **Yi Min Xie:** Writing – review & editing, Supervision, Methodology, Funding acquisition, Conceptualization.

Declaration of competing interest

The authors declare that they have no known competing financial interests or personal relationships that could have appeared to influence the work reported in this paper.

Acknowledgments

The authors gratefully acknowledge the financial support provided by the Australian Research Council (FL190100014). The authors would like to thank Robin Song, Dr. Zicheng Zhuang, Dr. Yunzhen He, and Yuanpeng Liu for their helpful advice on various technical issues examined in this paper.

Appendix. Implementation of VR sculpting

The VR sculpting system is implemented by a volumetric sculpting method based on sparse hashing techniques [57,58]. The system first divides the cubic workspace of 2 m × 2 m × 2 m around the designer into a voxel grid of 256 × 256 × 256. In the voxel grid, designers

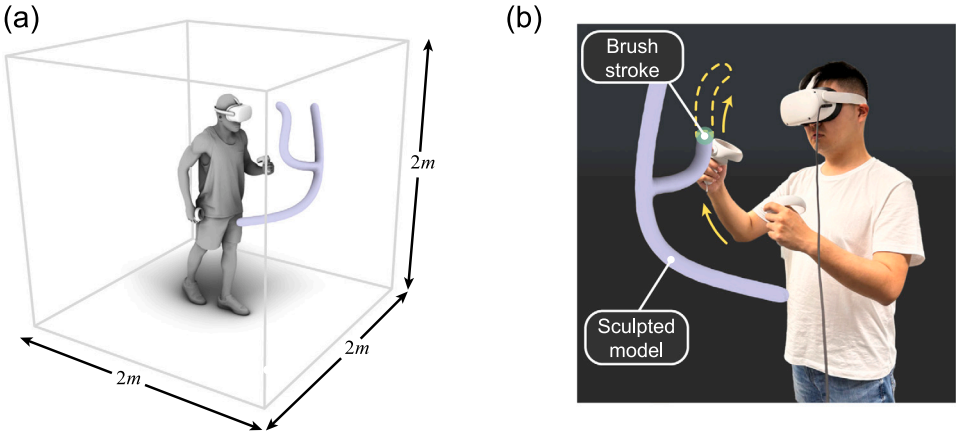

Fig. 11. (a) Visualization of a designer and the workspace in VR-BESO; (b) the brush stroke of VR sculpting.

can use the brush tool in the sculpting controller to draw 3D models. Specifically, after activating the brush tool, a spherical region in front of the virtual controller appears, representing the brush stroke, as shown in Fig. 11(a). The brush stroke size is adjustable by manipulating the thumbstick on the right controller. When the designer presses the controller trigger, the voxel nodal values within the brush stroke can be improved (drawing mode) or decreased (erasing mode). The nodal values in the workspace form a signed distance field (SDF). The values are then utilized to generate a mesh model via the marching cubes (MC) method [59]. Furthermore, pressing the right index trigger while waving the controller produces a tubular geometry that traces the moving path. Together, using the sculpting brush, designers can intuitively and flexibly design preferred 3D models [43,60]. More details of the sculpting brush can be found in [42].

The importing and exporting features mentioned in Section 2.1 are also integrated into the sculpting system. In order to allow users to edit imported models through VR Sculpting, the imported models need to be reconstructed to support further modifications [45]. In detail, these models are initially utilized to compute an SDF in the workspace [61]. Then, a 3D mesh model can be extracted from the scalar field using the MC method [59]. Since both the reconstructed model and the sculpted system use the SDF, designers can directly edit the former using the brush tool. After sculpting, designers can directly export the extracted mesh models in the OBJ format, facilitating further editing in the external CAD software.

Data availability

Data will be made available on request. The VR-BESO software can be downloaded from: https://doi.org/10.25439/rmt.25469278.v1.

References

[1] Bendsøe MP, Sigmund O. Topology optimization: Theory, methods, and applications. Springer Science & Business Media; 2013, http://dx.doi.org/10.1007/978-3-662-05086-6.

[2] Huang X, Xie YM. Evolutionary topology optimization of continuum structures: Methods and applications. John Wiley & Sons; 2010, http://dx.doi.org/10.1002/9780470689486.

[3] Li Y, Wu H, Xie X, Zhang L, Yuan PF, Xie YM. FloatArch: A cable-supported, unreinforced, and re-assemblable 3D-printed concrete structure designed using multi-material topology optimization. Addit Manuf 2024;81:104012. http://dx.doi.org/10.1016/j.addma.2024.104012.

[4] Xu T, Shen W, Lin X, Xie YM. Additively manufactured thermoplastic polyurethane (TPU) mold for concrete casting of complex structure. Rapid Prototyp J 2022;28(9):1717–30.

[5] Bi M, Tran P, Xia L, Ma G, Xie YM. Topology optimization for 3D concrete printing with various manufacturing constraints. Addit Manuf 2022;57:102982. http://dx.doi.org/10.1016/j.addma.2022.102982.

[6] Nguyen KC, Tran P, Nguyen HX. Multi-material topology optimization for additive manufacturing using polytree-based adaptive polygonal finite elements. Autom Constr 2019;99:79–90. http://dx.doi.org/10.1016/j.autcon.2018.12.005.

[7] Fu Y-F, Rolfe B, Chiu LNS, Wang Y, Huang X, Ghabraie K. Design and experimental validation of self-supporting topologies for additive manufacturing. Virtual Phys Prototyp 2019;14(4):382–94. http://dx.doi.org/10.1080/17452759.2019.1637023.

[8] Lai Y, Li Y, Liu Y, Chen P, Zhao L, Li J, et al. Application of bi-directional evolutionary structural optimization to the design of an innovative pedestrian bridge. AI Civ Eng 2024;3(1):9. http://dx.doi.org/10.1007/s43503-024-00027-5.

[9] Li Y, Lai Y, Lu G, Yan F, Wei P, Xie YM. Innovative design of long-span steel–concrete composite bridge using multi-material topology optimization. Eng Struct 2022;269:114838. http://dx.doi.org/10.1016/j.engstruct.2022.114838.

[10] Lai Y, Li Y, Huang M, Zhao L, Chen J, Xie YM. Conceptual design of long span steel-UHPC composite network arch bridge. Eng Struct 2023;277:115434. http://dx.doi.org/10.1016/j.engstruct.2022.115434.

[11] Li Y, Xie YM. Evolutionary topology optimization for structures made of multiple materials with different properties in tension and compression. Compos Struct 2021;259:113497. http://dx.doi.org/10.1016/j.compstruct.2020.113497.

[12] Li Y, Ding J, Zhang Z, Zhou X, Makvandi M, Yuan PF, et al. Practical application of multi-material topology optimization to performance-based architectural design of an iconic building. Compos Struct 2023;325:117603. http://dx.doi.org/10.1016/j.compstruct.2023.117603.

[13] Xie YM. Generalized topology optimization for architectural design. Archit Intell 2022;1(1):2. http://dx.doi.org/10.1007/s44223-022-00003-y.

[14] Yan X, Bao D, Zhou Y, Xie YM, Cui T. Detail control strategies for topology optimization in architectural design and development. Front Archit Res 2022;11(2):340–56. http://dx.doi.org/10.1016/j.foar.2021.11.001.

[15] Meng X, Xiong Y, Xie YM, Sun Y, Zhao Z-L. Shape–thickness–topology coupled optimization of free-form shells. Autom Constr 2022;142:104476. http://dx.doi.org/10.1016/j.autcon.2022.104476.

[16] Beghini LL, Beghini A, Katz N, Baker WF, Paulino GH. Connecting architecture and engineering through structural topology optimization. Eng Struct 2014;59:716–26. http://dx.doi.org/10.1016/j.engstruct.2013.10.032.

[17] Xu T, Lin X, Xie YM. Topology optimisation considering buckling in architectural design. In: Proceedings of IASS annual symposia, vol. 2023, International Association for Shell and Spatial Structures (IASS); 2023, p. 2422–9.

[18] Ma J, Gomaa M, Bao DW, Javan AR, Xie YM. PrintNervi–design and construction of a ribbed floor system in the digital era. J Int Assoc Shell Sp 2022;63(4):241–51. http://dx.doi.org/10.20898/j.iass.2022.017.

[19] Ma J, Li Z, Zhao Z-L, Xie YM. Creating novel furniture through topology optimization and advanced manufacturing. Rapid Prototyp J 2021;27(9):1749–58. http://dx.doi.org/10.1108/RPJ-03-2021-0047.

[20] Li Z, Lee T-U, Xie YM. Interactive structural topology optimization with subjective scoring and drawing systems. Comput Aided Des 2023;160:103532. http://dx.doi.org/10.1016/j.cad.2023.103532.

[21] Li Z, Lee T-U, Xie YM. Topology optimisation considering subjective preferences: current progress and challenges. In: Proceedings of IASS annual symposia, vol. 2023, International Association for Shell and Spatial Structures (IASS); 2023, p. 2430–40.

[22] Martínez J, Dumas J, Lefebvre S, Wei L-Y. Structure and appearance optimization for controllable shape design. ACM Trans Graph 2015;34(6):1–11.

[23] Navez T, Schmidt M-P, Sigmund O, Pedersen CB. Topology optimization guided by a geometrical pattern library. Struct Multidiscip Optim 2022;65(4):108.

[24] Zhang W, Wang Y, Du Z, Liu C, Youn S-K, Guo X. Machine-learning assisted topology optimization for architectural design with artistic flavor. Comput Methods Appl Mech Engrg 2023;413:116041. http://dx.doi.org/10.1016/j.cma.2023.116041.

[25] Zhang W, Wang Y, Youn S-K, Guo X. Machine learning powered sketch aided design via topology optimization. Comput Methods Appl Mech Engrg 2024;419:116651. http://dx.doi.org/10.1016/j.cma.2023.116651.

[26] Zhong S, Punpongsanon P, Iwai D, Sato K. Topology optimization with text-guided stylization. Struct Multidiscip Optim 2023;66(12):256. http://dx.doi.org/10.1007/s00158-023-03686-7.

[27] Oh S, Jung Y, Kim S, Lee I, Kang N. Deep generative design: Integration of topology optimization and generative models. J Mech Des 2019;141(11):111405. http://dx.doi.org/10.1115/1.4044229.

[28] Yan X, Xiong Y, Bao DW, Xie YM, Peng X. A multi-volume constraint approach to diverse form designs from topology optimization. Eng Struct 2023;279:115525. http://dx.doi.org/10.1016/j.engstruct.2022.115525.

[29] Loos S, Wolk Svd, Graaf Nd, Hekkert P, Wu J. Towards intentional aesthetics within topology optimization by applying the principle of unity-in-variety. Struct Multidiscip Optim 2022;65(7):185. http://dx.doi.org/10.1007/s00158-022-03288-9.

[30] Chen M, Zhao T, Zhang H, Luo S. A study of the influence of images on design creative stimulation. In: Social computing and social media. user experience and behavior. 2018, p. 3–18. http://dx.doi.org/10.1007/978-3-319-91521-0_1.

[31] Mueller CT, Ochsendorf JA. Combining structural performance and designer preferences in evolutionary design space exploration. Autom Constr 2015;52:70–82. http://dx.doi.org/10.1016/j.autcon.2015.02.011.

[32] Schiffer G, Schmidt M-P, Pedersen CBW, Carstensen JV. Interactive infill topology optimisation guided by user drawn patterns. Virtual Phys Prototyp 2024;19(1):e2361864. http://dx.doi.org/10.1080/17452759.2024.2361864.

[33] Ha DQ, Carstensen JV. Human-informed topology optimization: interactive application of feature size controls. Struct Multidiscip Optim 2023;66(3):59. http://dx.doi.org/10.1007/s00158-023-03512-0.

[34] Schiffer G, Ha DQ, Carstensen JV. Hitop 2.0: combining topology optimisation with multiple feature size controls and human preferences. Virtual Phys Prototyp 2023;18(1):e2268603. http://dx.doi.org/10.1080/17452759.2023.2268603.

[35] Wolfartsberger J. Analyzing the potential of virtual reality for engineering design review. Autom Constr 2019;104:27–37. http://dx.doi.org/10.1016/j.autcon.2019.03.018.

[36] Sigmund O, Petersson J. Numerical instabilities in topology optimization: a survey on procedures dealing with checkerboards, mesh-dependencies and local minima. Struct Optim 1998;16:68–75. http://dx.doi.org/10.1007/BF01214002.

[37] Zuo ZH, Xie YM. A simple and compact python code for complex 3D topology optimization. Adv Eng Softw 2015;85:1–11. http://dx.doi.org/10.1016/j.advengsoft.2015.02.006.

[38] Huang X, Xie YM. Convergent and mesh-independent solutions for the bi-directional evolutionary structural optimization method. Finite Elem Anal Des 2007;43(14):1039–49. http://dx.doi.org/10.1016/j.finel.2007.06.006.

[39] Wang B, Zhou Y, Zhou Y, Xu S, Niu B. Diverse competitive design for topology optimization. Struct Multidiscip Optim 2018;57:891–902. http://dx.doi.org/10.1007/s00158-017-1762-9.

[40] Xiong Y, Zhao Z-L, Lu H, Shen W, Xie YM. Parallel BESO framework for solving high-resolution topology optimisation problems. Adv Eng Softw 2023;176:103389. http://dx.doi.org/10.1016/j.advengsoft.2022.103389.
[41] Li Z, Lee TU, Xie YM. Vr-beso: a vr-based structural design tool. 2024, https://albertlidesign.gitbook.io/vr-beso. [Accessed 11 October 2024].
[42] Chen C-W, Hu M-C, Chu W-T, Chen J-C. A real-time sculpting and terrain generation system for interactive content creation. IEEE Access 2021;9:114914–28. http://dx.doi.org/10.1109/ACCESS.2021.3105417.
[43] Galyean TA, Hughes JF. Sculpting: An interactive volumetric modeling technique. ACM SIGGRAPH Comput Graph 1991;25(4):267–74. http://dx.doi.org/10.1145/127719.122747.
[44] Robert McNeel & Associates (TLM, Inc). Rhino - rhinoceros 3d. 2024, https://www.rhino3d.com. [Accessed 11 October 2024].
[45] Kazhdan M, Bolitho M, Hoppe H. Poisson surface reconstruction. In: Proceedings of the fourth eurographics symposium on geometry processing, vol. 7, no. 4. 2006, http://dx.doi.org/10.5555/1281957.1281965.
[46] Fu Y-F, Rolfe B, Chiu LNS, Wang Y, Huang X, Ghabraie K. SEMDOT: Smooth-edged material distribution for optimizing topology algorithm. Adv Eng Softw 2020;150:102921. http://dx.doi.org/10.1016/j.advengsoft.2020.102921.
[47] Fu Y-F, Rolfe B, Chiu LNS, Wang Y, Huang X, Ghabraie K. Smooth topological design of 3D continuum structures using elemental volume fractions. Comput Struct 2020;231:106213. http://dx.doi.org/10.1016/j.compstruc.2020.106213.
[48] Li Z, Lee T-U, Yao Y, Xie YM. Smoothing topology optimization results using pre-built lookup tables. Adv Eng Softw 2022;173:103204. http://dx.doi.org/10.1016/j.advengsoft.2022.103204.
[49] Andreassen E, Clausen A, Schevenels M, Lazarov BS, Sigmund O. Efficient topology optimization in MATLAB using 88 lines of code. Struct Multidiscip Optim 2011;43:1–16. http://dx.doi.org/10.1007/s00158-010-0594-7.
[50] Ferrari F, Sigmund O. A new generation 99 line matlab code for compliance topology optimization and its extension to 3D. Struct Multidiscip Optim 2020;62:2211–28. http://dx.doi.org/10.1007/s00158-020-02629-w.
[51] Intel Corporation. oneMKL PARDISO - Parallel direct sparse solver interface. 2024, https://www.intel.com/content/www/us/en/docs/onemkl/developer-reference-c/2023-0/onemkl-pardiso-parallel-direct-sparse-solver-iface.html. [Accessed 11 October 2024].
[52] Gaël G, Beno J, et al. Eigen v3. 2024, http://eigen.tuxfamily.org. [Accessed 11 October 2024].
[53] Unity Technologies. Unity real-time development platform. 2024, https://www.unity.com. [Accessed 11 October 2024].
[54] Meta. Meta quest 3: new mixed reality vr headset. 2023, https://www.meta.com/au/quest/quest-3/. [Accessed 11 October 2024].
[55] Clausen A, Aage N, Sigmund O. Topology optimization with flexible void area. Struct Multidiscip Optim 2014;50:927–43. http://dx.doi.org/10.1007/s00158-014-1109-8.
[56] Cui C, Ohmori H, Sasaki M. Computational morphogenesis of 3D structures by extended ESO method. J Int Assoc Shell Sp 2003;44(1):51–61.
[57] Lefebvre S, Hoppe H. Perfect spatial hashing. ACM Trans Graph 2006;25(3):579–88. http://dx.doi.org/10.1145/1141911.1141926.
[58] Nießner M, Zollhöfer M, Izadi S, Stamminger M. Real-time 3D reconstruction at scale using voxel hashing. ACM Trans Graph 2013;32(6):1–11. http://dx.doi.org/10.1145/2508363.2508374.
[59] Lorensen WE, Cline HE. Marching cubes: a high resolution 3D surface construction algorithm. In: Seminal graphics: pioneering efforts that shaped the field. Association for Computing Machinery; 1998, p. 347–53. http://dx.doi.org/10.1145/37402.37422.
[60] Ferley E, Cani M-P, Gascuel J-D. Practical volumetric sculpting. Visual Comput 2000;16(8):469–80. http://dx.doi.org/10.1007/PL00007216.
[61] Botsch M, Kobbelt L, Pauly M, Alliez P, Lévy B. Polygon mesh processing. CRC Press; 2010, http://dx.doi.org/10.1201/b10688.